

Effect of Na_2CO_3 and CaCO_3 on deep dephosphorization by the direct reduction of high-phosphorus oolitic hematite

Hongda Xu ¹, Rui Li ², Jue Kou ¹, Xiaojin Wen ¹, Jun Zhang ¹, Chao Geng ³, Tichang Sun ¹

¹ School of Civil and Resource Engineering, University of Science and Technology Beijing, Beijing 100083, China

² Changsha Research Institute of Mining and Metallurgy Company Limited, Hunan Changsha 410012, China

³ School of Civil Engineering, North China University of Technology, Beijing 100144, China

Corresponding authors: koujue@ustb.edu.cn (Jue Kou), gengchao1988@yeah.net (Chao Geng)

Abstract: The direct reduction–magnetic separation process based on coal is considered to be one of the most important methods that can effectively utilize high-phosphorus oolitic hematite. In this study, the mechanism of the effects of CaCO_3 and Na_2CO_3 on the dephosphorization of high-phosphorus oolitic hematite during the direct reduction process was investigated using X-ray diffraction (XRD), scanning electron microscope (SEM) and energy dispersive spectrometer (EDS). The results showed that Na_2CO_3 and CaCO_3 reacted with Al_2O_3 and SiO_2 during the direct reduction process, inhibited the generation of hercynite (FeAl_2O_4) and fayalite (Fe_2SiO_4), and promoted the reduction of metallic iron (Fe). Furthermore, the reaction inhibited the reduction of apatite and prevented the generation of FeP_2 . Na_2CO_3 could change the form of phosphorus in the gangue from $\text{Ca}_3(\text{PO}_4)_2$ to $\text{Na}_2\text{Ca}_4(\text{PO}_4)_2\text{SiO}_4$. Increasing the dosages of Na_2CO_3 and CaCO_3 in the dephosphorization agent and increasing the content of Na_2CO_3 in the dephosphorization agent were beneficial to the growth of metallic iron particles, and increasing the dosage of Na_2CO_3 , CaCO_3 in the dephosphorization agent had more significant effects on metallic iron particles than increasing the content of Na_2CO_3 in the dephosphorization agent. The research conducted in this study is expected to provide a basis for the effective exploitation of complex and refractory iron ores.

Keywords: high-phosphorus oolitic hematite, deep dephosphorization, direct reduction, Na_2CO_3 , CaCO_3

1. Introduction

With the continuous consumption of easy-to-treat high-grade iron ores, the effective utilization of refractory iron ores has gradually become a popular research topic (Anameric and Kawatra, 2007; Bao et al., 2021; Pownceby et al., 2019; Roy et al., 2020; Sun et al., 2015). High-phosphorus oolitic hematite (HPOH) is a typical complex and refractory iron ore with large reserves and widespread distribution and has a special oolitic structure with fine grain distribution between iron minerals and gangue and a high phosphorus content (P content) (Jin et al., 2021; Wu et al., 2023; Wu et al., 2022; Zhang and Luo, 2017). Numerous studies have been conducted on this challenging type of ore; however, it is difficult to obtain an iron concentrate with a low P content using conventional methods (Nunes et al., 2012; Omran et al., 2015; Sun et al., 2017; Tang et al., 2015; Xiao and Zhou, 2019). Such flotation can only obtain iron ore concentrates with a P content of 0.14% (Chen et al., 2023), although acid or alkaline leaching showed excellent dephosphorization, with leach products containing 0.1% phosphorus and more than 90% dephosphorization; however, the leaching reagent is expensive and the leaching liquor is untreated, causing environmental pollution (Delvasto et al., 2008; Pan et al., 2022; Shen et al., 2013; Wang et al., 2017; Zhang et al., 2019).

Studies have demonstrated that the coal-based direct reduction–magnetic separation process transforms the ore structure and allows the phosphorus content of the product to be reduced to less than 0.1% while achieving a powdery reduced iron (PRI) product of good quality (Wu et al., 2023; Wu et al., 2021; Yu et al., 2014; Yu et al., 2015). Although this method has the advantages of high resource utilization, simple processing, and simultaneous enhancement of iron and phosphorus reduction, the

direct reduction process requires the addition of Ca- or Na-containing dephosphorization agents (Wu et al., 2022; Wu et al., 2022). The calcium-containing dephosphorization agent represented by limestone has the advantage of lower price, but it needs to add 30% of HPOH. Although the amount of Na-containing dephosphorization agent represented by industrial production Na_2CO_3 is low, the price of industrial production Na_2CO_3 is more than ten times that of limestone (Xu et al., 2023; Yu et al., 2016). Hence, some scholars have proposed a combination of CaCO_3 and Na_2CO_3 as a dephosphorization agent to effectively reduce the dosage; however, the mechanism for the dosage of CaCO_3 and Na_2CO_3 as a dephosphorization agent has not yet been clarified (Wu et al., 2021; Wu et al., 2022; Wu et al., 2022).

In this study, based on the response surface method and Box-Behnken design (RSM-BBD) experimental design methodology, we conducted research on compound dephosphorization agent conditions. The mechanism of the combined dephosphorization agent containing Na_2CO_3 and CaCO_3 was illustrated by X-ray diffraction (XRD) analysis and scanning electron microscope energy spectroscopy (SEM-EDS). The research conducted in this study is expected to provide a basis for the effective exploitation of complex and refractory iron ores.

2. Materials and methods

2.1. Materials

HPOP was sampled from Hubei Province, China, and the chemical multi-elemental analyses are presented in Tab. 1. The sampled HOPH contained 44.38% of total iron and 0.92% of phosphorus, and the content of gangue components exceeded 25%, indicating that HOPH cannot be used without sorting. As shown in Fig. 1, HPOH is composed of hematite, quartz, apatite, and chlorite. Figs. 2(a) and (b) show the typical oolitic structure of HPOP and the distribution of Fe, Ca, P, and Si in HPOP, respectively, indicating that HOPH has a typical oolitic structure and a close Fe-P relationship.

Analytically pure CaCO_3 and Na_2CO_3 were obtained from Sinopharm Chemical Reagent Co. Ltd., China, and used as additives.

Anthracite containing 81.46% fixed carbon, 11.28% ash content, and 6.88% volatile matter was the reductant in this project.

Tab. 1. Chemical compositions of HPOH/Wt. %

Component	TFe	SiO_2	Al_2O_3	MgO	CaO	S	P	MnO
HPOH	44.38	16.85	9.38	0.59	3.61	0.049	0.92	0.20

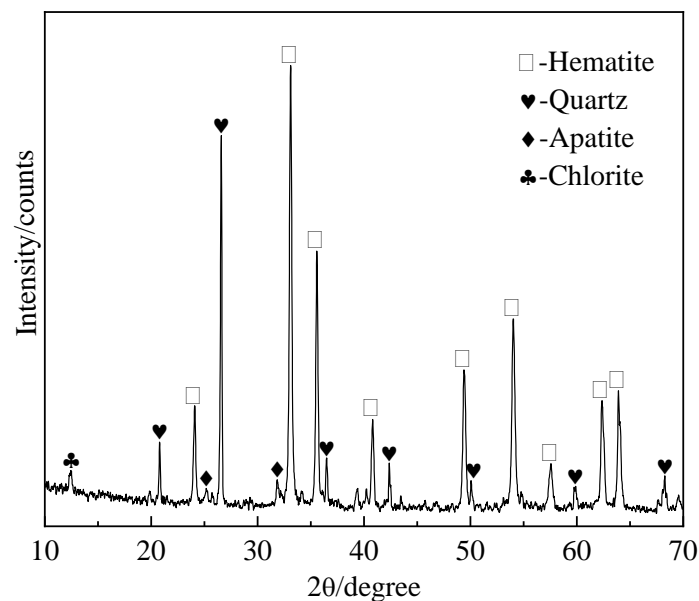


Fig. 1. The mineral compositions of HPOP

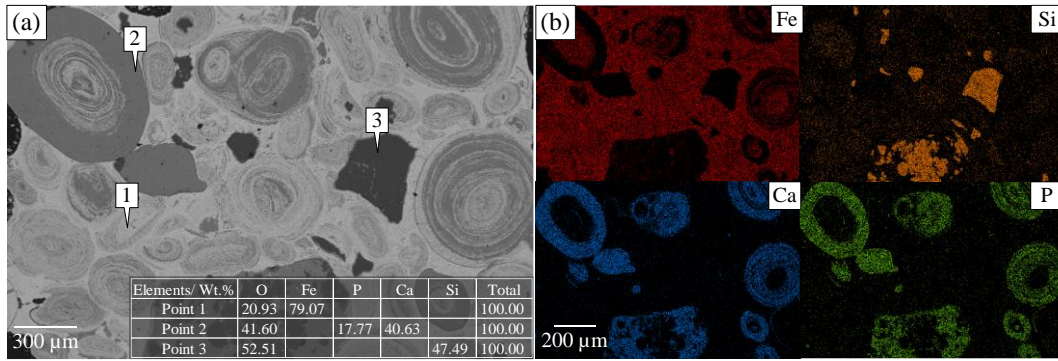


Fig. 2. Microscopic characteristics of HPOH: (a) SEM photograph; (b) distribution of Fe, Ca, P, and Si elemental surface in (a)

2.2. Direct reduction and magnetic separation

A total of 40 g of HPOP was mixed with specific proportions of anthracite and the dephosphorization agent. The mixture was then charged into clay crucibles with lids. The temperature of the muffle furnace was increased to the target temperature of 1200 °C at a heating rate of 10 °C/min and the mixture was placed into a furnace muffle to allow for reduction for 70 min. The crucibles were then removed from the furnace and allowed to cool naturally to room temperature. The reduced products were then subjected to stage grinding and magnetic separation. In the first stage, 75.43% of the particles were ground to 74 μm. The magnetically separated and weakly magnetic titanium concentrates were separated using a Davis magnetic tube with a magnetic field strength of 111.41 kA/m. Subsequently, the magnetic concentrate was ground to 45 μm, accounting for 60.19%. The directly reduced iron and gangue were separated using the same magnetic separation tube at a magnetic field intensity of 95.49 kA/m. The final magnetic product obtained was called the direct reduction iron. A detailed schematic of direct reduction and magnetic separation is shown in Fig. 3.

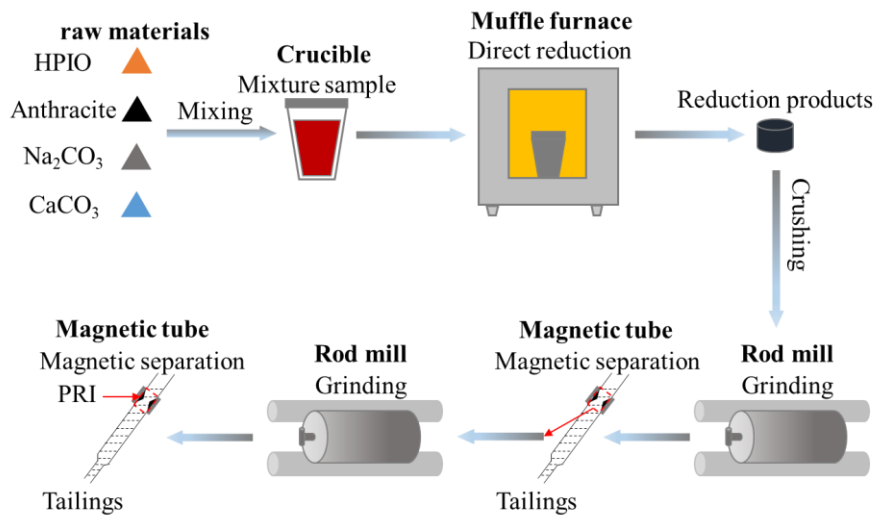


Fig. 3. Schematic diagram of the direct reduction and magnetic separation

2.3. Experimental design

Based on the RSM-BBD, this experiment was conducted to perform optimization research on compound dephosphorization agent conditions. The experimental parameters and their values are listed in Tab.2. Referring to the results reported in References (Wu et al., 2021; Yu et al., 2014; Xu et al., 2023; Li et al., 2012; Li et al., 2012), the dosages of anthracite and the combined dephosphorization agent were both 10–20%, and the proportion of Na_2CO_3 in the combined dephosphorization agent was 10–40%. Based on the experimental design of the RSM-BBD, we investigated the effect of the dosage of the compound dephosphorization agent, the influence of the proportion of $\text{Na}_2\text{CO}_3:\text{CaCO}_3$ on the extraction of iron

and the reduction of phosphorus by the combined dephosphorization agent. Furthermore, we examined the effect of the reductant dosage on the extraction of iron and the reduction of phosphorus by the combined dephosphorization agent.

Tab.2. RSM-BBD experimental factors and levels

Factors	Unit	-1	0	1
Dosage of the dephosphorization agent-x ₁	wt%	10	15	20
Dosage of Na ₂ CO ₃ in the dephosphorization agent-x ₂	wt%	10	25	40
Dosage of anthracite-x ₃	wt%	10	15	20

2.4. Characterization

The TFe grade and P content of the product were determined using the methods described in GB/T6730.65-2009 and GB/T6730.18-2006, respectively. Mineralogical characteristics were examined using XRD (RIGAKU, D/Max 2500, Japan). The microstructure and distribution behavior of iron and P in the reduced products were observed using SEM-EDS (VEGA 3 XHU, Tescan, Czech Republic) to reveal the elemental distribution in the roasted product. The amount of iron recovered from PRI was calculated as follows:

$$\varepsilon = \frac{m_b \times \beta_b}{m_a \times \beta_{Fe}} \times 100\% \quad (1)$$

where ε is the iron recovered from PRI; m_a and m_b represent the masses of HPOP and PRI, respectively; and β_{Fe} and β_b are the iron grades of HPOP and powdery reduction iron, respectively.

In this study, the TFe in the PRI was more than 90%, indicating that the Na₂CO₃ and CaCO₃ dosage or ratio and anthracite dosage had a remarkably insignificant effect on TFe; hence, they are not discussed here.

3. Results and discussion

3.1. Thermodynamic analysis

According to the metallurgical theory, the CO provided by coal is mainly generated by the Boudouard reaction. This reaction provides an atmosphere for the reduction of iron oxides to metallic iron. In the process of direct deep dephosphorization of HPOP, to avoid a high P content in the metallic iron, the addition of a dephosphorization agent generally inhibits the reduction of P-containing gangue. In this study, the important reactions possibly involved in the direct reduction reaction process of the dephosphorizer were thermodynamically analyzed using the reaction module in FactSage 8.3 software, and the results are shown in Fig. 4. Na₂CO₃ and CaCO₃ are simplified as Na₂O and CaO, respectively.

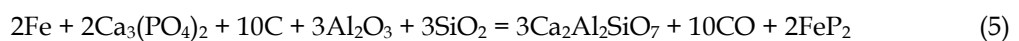
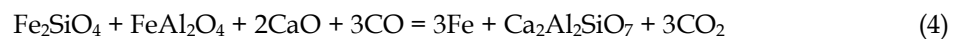
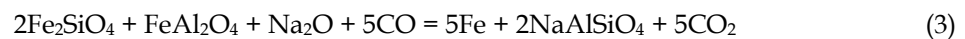
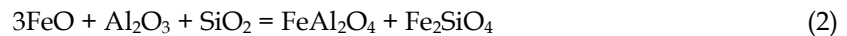


Fig. 4 shows that Eqs. (2)–(8) can react at a reduction temperature of 1200 °C. Without the addition of Na₂CO₃ and CaCO₃, Fe_xO reacts with Al₂O₃ and SiO₂ (Eq. (2)) to form FeAl₂O₄ and Fe₂SiO₄, respectively, whereas Fe reacts with Ca₃(PO₄)₂ (Eq. (5)) to form FeP₂. When Na₂CO₃ and CaCO₃ were added, the Na₂CO₃ and CaCO₃ decomposition products Na₂O and CaO react with FeAl₂O₄ and Fe₂SiO₄ to form Fe (Eqs. (3) and (4)) and Na₂O and CaO react with SiO₂ and Al₂O₃ (Eqs. (6), (7) and (8)).

Therefore, Eqs. (3) and (4) are more probable than Eqs. (2); Eqs. (6), (7), and 8 are more probable than Eq. (5) at the reduction temperature of 1200 °C.

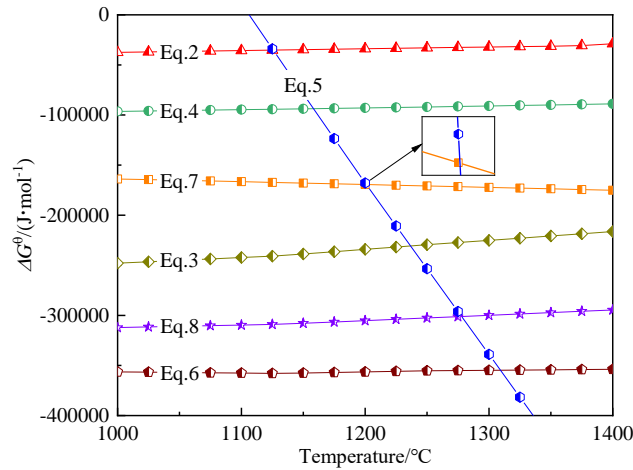


Fig. 4. Thermodynamic results

3.2. Effect of the dosage of the dephosphorization agent

3.2.1. Effect of the dosage of the dephosphorization agent Index of PRI

The influence of the dosage of Na_2CO_3 and CaCO_3 on the index of PRI was studied under the conditions of a reductant agent dosage of 15%, $\text{Na}_2\text{CO}_3:\text{CaCO}_3$ of 1:3, and dephosphorization dosages of 6.6%, 10.0%, 15.0%, 20.0%, and 23.4% of Fe recovery and P content in PRI, as shown in Fig. 5.

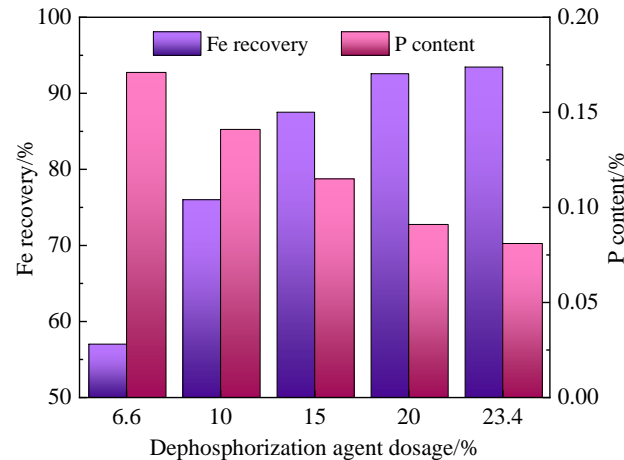


Fig. 5. Effect of the dephosphorization agent dosage on PRI

Fig. 5 shows that the dosage of the dephosphorization agent has a significant effect on Fe recovery and P content in PRI. The dosage of the dephosphorization agent was increased from 6.6% to 20%, the Fe recovery in PRI was significantly increased from 67.68% to 91.56%, and the P content was considerably reduced from 0.171% to 0.115%. The dosage of the dephosphorization agent was increased from 20% to 23.4%, Fe recovery was slightly increased from 91.56% to 93.45%, and the P content was considerably reduced from 0.115% to 0.081%. This indicates that, when the anthracite dosage and $\text{Na}_2\text{CO}_3:\text{CaCO}_3$ ratio are fixed, increasing the dosage of the dephosphorization agent is beneficial for improving Fe recovery and reducing the P content in PRI.

3.2.2. Mineral transformation

To investigate the effect of the dephosphorization agent dosage on the mineral composition of direct reduction products, the direct reduction products described above were analyzed using XRD, and the results are shown in Fig. 6.

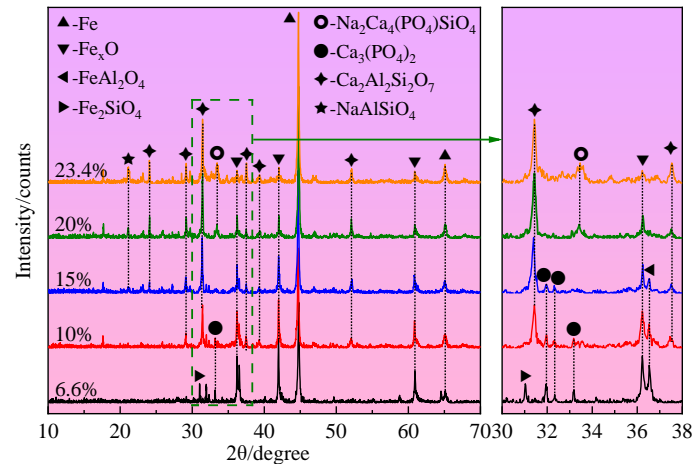


Fig. 6. XRD pattern of direct reduction products

Fig. 6 shows the significant effect of the dephosphorization agent dosage on the composition and content of iron minerals in the direct reduction products. At a dephosphorization agent dosage of 6.6%, the iron minerals in reduction products were primarily metallic iron (Fe), wüstite (Fe_xO), hercynite (FeAl_2O_4), and fayalite (Fe_2SiO_4). Furthermore, hercynite (FeAl_2O_4) and fayalite (Fe_2SiO_4) were observed in the iron mineral owing to the occurrence of Eq. 2. When the dephosphorization agent dosage was increased to 10%, the diffraction peak of fayalite (Fe_2SiO_4) in the reduction product disappeared. The raw ore properties indicated that the content of SiO_2 was higher than that of Al_2O_3 , indicating that the dephosphorization agent preferentially reacted with SiO_2 . When the dephosphorization agent dosage was increased to 20%, the diffraction peaks of hercynite (FeAl_2O_4) disappeared, the content of wüstite (Fe_xO) gradually decreased, and the content of metallic iron (Fe) gradually increased with an increase in the dephosphorization agent dosage. This indicates that an increase in the dephosphorization agent dosage is beneficial for the occurrence of reactions in Eqs. 3 and 4 and inhibition of the reaction in Eq. 5. Fig. 5 shows that increasing the amount of the dephosphorization agent can inhibit hercynite (FeAl_2O_4) and fayalite (Fe_2SiO_4), and this is beneficial for improving Fe recovery.

Fig. 6 shows that the dephosphorization agent dosage has a significant effect on the composition and content of gangue in the direct reduction product. At a dephosphorization agent dosage of 6.6%, the gangue was primarily composed of apatite ($\text{Ca}_3(\text{PO}_4)_2$) and gehlenite ($\text{Ca}_2\text{Al}_2\text{Si}_7\text{O}_7$). As the dephosphorization agent dosage was increased, the content of apatite ($\text{Ca}_3(\text{PO}_4)_2$) gradually decreased and that of gehlenite ($\text{Ca}_2\text{Al}_2\text{Si}_7\text{O}_7$) gradually increased. As the dephosphorization agent dosage was increased to 15%, nepheline ($\text{NaAlSi}_3\text{O}_8$) appeared in the reduction product. At a dephosphorization agent dosage of 20%, the diffraction peaks of apatite ($\text{Ca}_3(\text{PO}_4)_2$) in the gangue disappeared, whereas those of $\text{Na}_2\text{Ca}_4(\text{PO}_4)_2\text{SiO}_4$ in the gangue appeared. FactSage 8.3 software in the FactPS and FToxid databases does not include $\text{Na}_2\text{Ca}_4(\text{PO}_4)_2\text{SiO}_4$; therefore, $\text{Na}_2\text{Ca}_4(\text{PO}_4)_2\text{SiO}_4$ was simplified to $\text{Na}_2\text{SiO}_3 + \text{Ca}_3(\text{PO}_4)_2 + \text{CaO}$, and Eq. 8 can be written as $\text{Na}_2\text{O} + \text{CaO} + \text{SiO}_2 + \text{Ca}_3(\text{PO}_4)_2 \rightarrow \text{Na}_2\text{Ca}_4(\text{PO}_4)_2\text{SiO}_4$, indicating that Na_2CO_3 and CaCO_3 change the form of the phosphorus. Furthermore, the results showed that an increase in the amount of the dephosphorization agent led to the occurrence of reactions in Eqs. 6, 7, and 8 simultaneously.

3.2.3. Microstructure evolution

Because XRD only clarifies the mineral composition of the reduction products, the impact of dephosphorization agent dosage on the microstructure of direct reduction products could not be clarified. Therefore, SEM-EDS was used to analyze the direct reduction products described above, and the results are shown in Fig. 7.

Fig. 7 shows that the dephosphorization agent dosage has a significant effect on the morphology of metallic iron particles present in the direct reduction product. An increase in the dephosphorization agent dosage from 6.6% to 23.4% resulted in significantly larger sizes of metallic iron particles, indicating that an increase in the dosage of the dephosphorization agent was favorable to the growth of

metallic iron particles. At a dephosphorization agent dosage of 6.6%, wüstite and hercynite were clearly observed in reduction products; however, small amounts of iron mineral particles that were not reduced to metallic iron were also observed, such as point 1. As the dephosphorization agent dosage was increased to 20%, hercynite disappeared from the reduction product. This indicates that increasing the dephosphorization agent dosage is beneficial in transforming iron minerals to metallic iron.

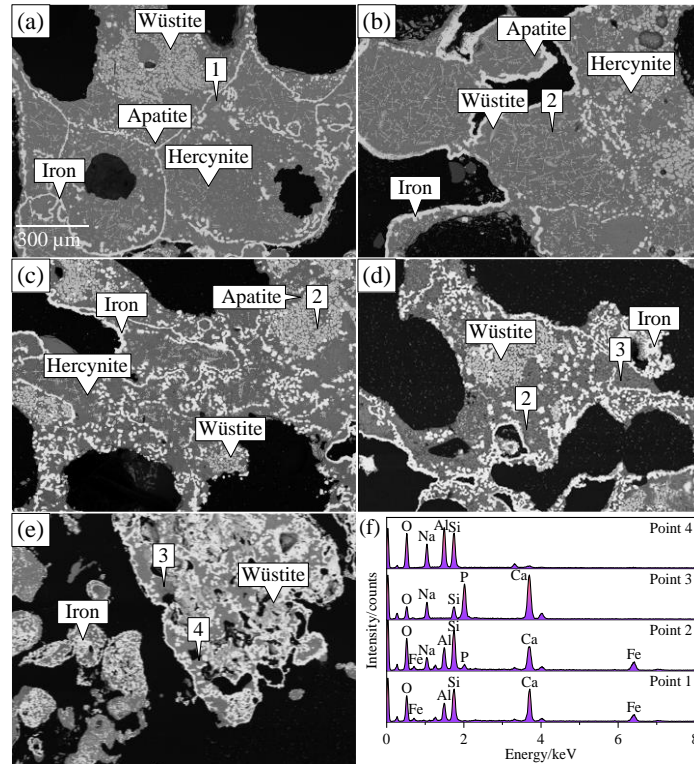


Fig. 7. Microscopic characteristics of reduction products at varying dephosphorization agent dosages: (a) 6.6%; (b) 10%; (c) 15%; (d) 20%; and (e) 23.4%. (f) Energy spectrum in (a)–(e)

Fig. 7 shows that the dephosphorization agent dosage has a significant effect on the form of phosphorus present in the direct reduction products. At a dosage of 6.6%, the phosphorus-containing gangue was mainly dominated by apatite, and, at a dosage of 10%, the phosphorus-containing gangue was mainly dominated by apatite and point 2 minerals. Moreover, a small amount of point 2 minerals also existed in iron mineral particles. As the dephosphorization agent dosage was increased to 20%, the phosphorus-containing gangue was mainly dominated by point 2 and 3 minerals. Furthermore, according to the composition and content of point 3 minerals, which were the products generated by the reaction between $\text{Ca}_3(\text{PO}_4)_2$, Na_2O , and SiO_2 , point 3 minerals were presumed to be $\text{Na}_2\text{Ca}_4(\text{PO}_4)_2\text{SiO}_4$. At a dosage of 23.4%, the phosphorus-containing gangue, such as point 2, disappeared from the reduction product and phosphorus-free gangue, such as point 4, appeared, indicating the transformation of the form of phosphorus.

The combined results of Figs. 6 and 7 indicate that, with an increase in the dosage of the dephosphorization agent, the decomposition products of the dephosphorization agent, that is, Na_2O and CaO , reacted with Al_2O_3 and SiO_2 in HOPH, inhibited hercynite (FeAl_2O_4) and fayalite (Fe_2SiO_4), and promoted the generation of metallic iron (Fe). Furthermore, the reaction in Eq. 5 was inhibited, and the generation of FeP_2 was efficiently prevented. Therefore, phosphorus present in the gangue was changed from $\text{Ca}_3(\text{PO}_4)_2$ to $\text{Na}_2\text{Ca}_4(\text{PO}_4)_2\text{SiO}_4$, which changed the composition of the gangue while also being beneficial for the growth of iron particles.

3.3. Effect of Na_2CO_3 and CaCO_3 ratio

3.3.1. PRI index

The influence of the Na_2CO_3 : CaCO_3 ratio on the PRI index was investigated. Under the conditions of

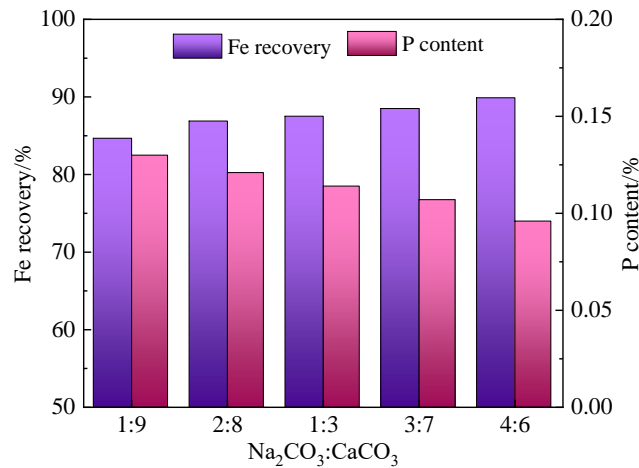


Fig. 8. Effect of the Na₂CO₃ and CaCO₃ ratio on PRI

15% reductant dosage and 15% dephosphorization agent dosage, the Fe recovery and P content of PRI with Na₂CO₃:CaCO₃ ratios of 1:9, 2:8, 1:3, 3:7, and 4:6 are shown in Fig. 8.

Fig. 8 shows that the Na₂CO₃:CaCO₃ ratio has a significant effect on the Fe recovery and P content in PRI. At Na₂CO₃:CaCO₃=1:9, Fe recovery was 84.67% and the P content was 0.130%. With an increase in the proportion of Na₂CO₃ in the dephosphorization agent, Fe recovery gradually increased and the P content gradually reduced. At Na₂CO₃:CaCO₃=4:6, Fe recovery was 90.71% and the P content was 0.096%. This means that, under the conditions of anthracite dosage and a fixed ratio of Na₂CO₃:CaCO₃, which increased the dosage of the dephosphorization agent, it is beneficial for increasing Fe recovery and reducing the P content in PRI.

3.3.2. Mineral transformation

To investigate the effect of the Na₂CO₃:CaCO₃ ratio on the mineral composition of direct reduction products, the abovementioned direct reduction products were analyzed by XRD, and the results are shown in Fig. 9.

Fig. 9 shows that the Na₂CO₃:CaCO₃ ratio has a significant effect on the composition and content of iron minerals in the direct reduction products. At Na₂CO₃:CaCO₃=1:9, the iron minerals in the reduction product were primarily metallic iron (Fe), wüstite (Fe_xO), and hercunite (FeAl₂O₄), whereas the presence of hercunite (FeAl₂O₄) in the reduction product was owing to the occurrence of the reaction in Eq. 2.

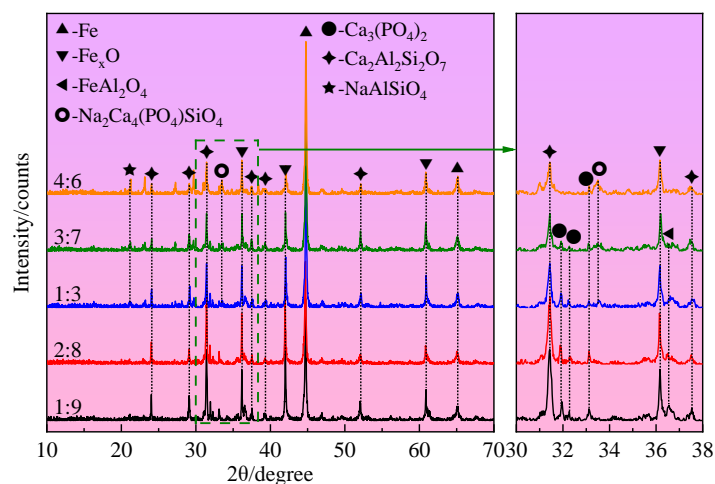


Fig. 9. XRD patterns of direct reduction products

Furthermore, the absence of fayalite (Fe₂SiO₄) in the reduction product indicates the preferential reaction of the dephosphorization agent with SiO₂. With a gradual increase in the Na₂CO₃ ratio and a

gradual decrease in the CaCO_3 ratio, the contents of wüstite (Fe_xO) and hercunite (FeAl_2O_4) gradually decreased and that of metallic iron (Fe) gradually increased. At $\text{Na}_2\text{CO}_3:\text{CaCO}_3=4:6$, the diffraction peaks of hercunite (FeAl_2O_4) disappeared, which was caused by a gradual decrease of the reaction in Eq. 4 and the completion of the reaction in Eq. 3. Fig. 4 shows that the reaction in Eq. 3 requires a lower Gibbs free energy. It also shows that the ability of Na_2O to promote the conversion of hercunite (FeAl_2O_4) to metallic iron (Fe) is better than that of CaO . Combined with Fig. 8, shows that the increase in the Na_2O ratio is more beneficial for improving Fe recovery when the dosage of the dephosphorization agent is fixed.

Fig. 9 shows that the $\text{Na}_2\text{CO}_3:\text{CaCO}_3$ ratio significantly affects the composition and content of gangue in the direct reduction products. At $\text{Na}_2\text{CO}_3:\text{CaCO}_3=1:9$, the gangue was primarily composed of apatite ($\text{Ca}_3(\text{PO}_4)_2$) and gehlenite ($\text{Ca}_2\text{Al}_2\text{SiO}_7$), and the diffraction peaks of apatite ($\text{Ca}_3(\text{PO}_4)_2$) and gehlenite ($\text{Ca}_2\text{Al}_2\text{SiO}_7$) gradually decreased with a gradual increase in the proportion of Na_2CO_3 and a gradual decrease in the proportion of CaCO_3 . At $\text{Na}_2\text{CO}_3:\text{CaCO}_3=1:3$, the diffraction peaks of sodium feldspar (NaAlSiO_4) and $\text{Na}_2\text{Ca}_4(\text{PO}_4)_2\text{SiO}_4$ appeared in the reduction product. As the ratio of Na_2CO_3 gradually increased and that of CaCO_3 gradually decreased, the contents of sodium feldspar (NaAlSiO_4) and $\text{Na}_2\text{Ca}_4(\text{PO}_4)_2\text{SiO}_4$ in the reduction product increased. This was caused by a gradual decrease in CaO and a gradual increase in Na_2O , which caused a gradual decrease of the reaction in Eq. 7 and a gradual increase of the reaction in Eqs. 6 and 8, thereby inhibiting the progress of the reaction in Eq. 5.

3.3.3. Microstructure evolution

As XRD can only define the mineral composition in the reduction products, it cannot determine the effect of the $\text{Na}_2\text{CO}_3:\text{CaCO}_3$ ratio on the microstructure of the direct reduction products. Therefore, SEM-EDS was used to analyze the abovementioned direct reduction products, and the results are shown in Fig. 10.

Fig. 10 shows that the $\text{Na}_2\text{CO}_3:\text{CaCO}_3$ ratio has a significant effect on the morphology of metallic iron particles present in the direct reduction products. When the $\text{Na}_2\text{CO}_3:\text{CaCO}_3$ ratio was increased from 1:9 to 4:6, the size of metallic iron particles significantly increased, indicating that an increase in the Na_2CO_3 ratio is beneficial to the growth of metallic iron particles. At $\text{Na}_2\text{CO}_3:\text{CaCO}_3=1:9$, the reduction products were wüstite and hercunite, along with a small number of iron mineral particles in the minerals that were not reduced to metallic iron, such as points 1 and 2. At $\text{Na}_2\text{CO}_3:\text{CaCO}_3=1:3$, the size of metallic iron particles in the reduction product significantly increased. At $\text{Na}_2\text{CO}_3:\text{CaCO}_3=4:6$, hercunite disappeared from the reduction product, indicating that increasing the content of Na_2CO_3 in the dephosphorization agent is beneficial to the transformation of iron minerals to metallic iron and also to the growth of metallic iron particles.

Fig. 10 shows that $\text{Na}_2\text{CO}_3:\text{CaCO}_3$ ratio has some effect on the form of phosphorus present in the direct reduction products. For $\text{Na}_2\text{CO}_3:\text{CaCO}_3 \leq 1:3$, the phosphorus-containing gangue was mainly dominated by apatite and minerals such as point 2, and a small number of iron minerals was present in point 2. At $\text{Na}_2\text{CO}_3:\text{CaCO}_3 > 1:3$, the phosphorus-containing gangue was mainly dominated by minerals such as apatite, points 2 and 3, whereas the composition and content of point 3 minerals indicated that the products were mainly generated by the reaction between apatite, Na_2O , and SiO_2 .

The combined results of Figs. 9 and 10 indicate that Na_2O reacts with Al_2O_3 and SiO_2 rather than CaO , and Fig. 4 also shows that Na_2O requires less energy to react with Al_2O_3 and SiO_2 than with CaO . A comparison between Figs. 5 and 8, and between Figs. 7 and 10 showed that increasing the dephosphorization agent with a fixed $\text{Na}_2\text{CO}_3:\text{CaCO}_3$ ratio or increasing the content of Na_2CO_3 in the dephosphorization agent with a fixed dephosphorization agent dosage had the same pattern of influence on the Fe recovery and P content of PRI and metallic iron particles in the reduced product; however, the former influence was more pronounced.

3.4. Effect of dephosphorization agent and reductant interaction on iron extraction and phosphorus reduction

To further investigate the interaction between Na_2CO_3 and CaCO_3 , under the conditions of $\text{Na}_2\text{CO}_3:\text{CaCO}_3=1:3$, we investigated the effect of anthracite dephosphorization agent dosages on Fe recovery and P content, respectively. Furthermore, under the condition of a dephosphorization agent

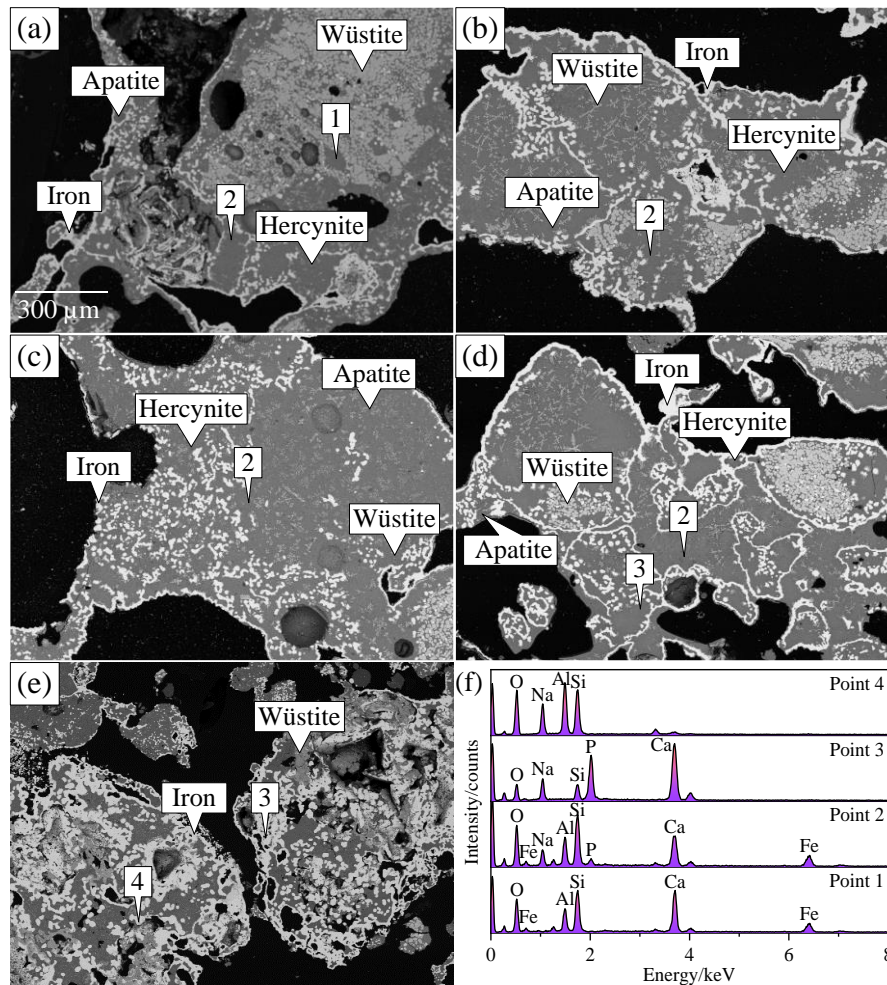


Fig. 10. Microscopic characteristics of reduction products at varying Na_2CO_3 and CaCO_3 ratio dosages: (a) 1:9; (b) 2:8; (c) 1:3; (d) 3:7; and (e) 4:6, (f) Energy spectrum in (a)–(e)

dosage of 15%, we investigated the effect of anthracite dosage and the ratio of Na_2CO_3 : CaCO_3 on Fe recovery and P content, respectively, and the results were shown in Fig. 11.

Figs. 11(a) and (c) show that increasing the dosage of the dephosphorization agent, Na_2CO_3 in the dephosphorization agent, and reductant improved Fe recovery. Under the same dosage of the reductant, increasing the dosage of the dephosphorization agent had a greater effect on Fe recovery than increasing the dosage of Na_2CO_3 in the dephosphorization agent.

Figs. 11 (b) and (d) show that increasing the dosage of the dephosphorization agent and Na_2CO_3 in the dephosphorization agent as well as reducing the dosage of anthracite gradually decreased the P content. Under the same dosage of the reductant, increasing the content of Na_2CO_3 in the dephosphorization agent had a more significant effect on the P content than increasing the dosage of the dephosphorization agent.

To further investigate the effect of reductant dosage on the PRI index, at a dephosphorization agent dosage of 15% and Na_2CO_3 : CaCO_3 =1:3, the effects of anthracite dosages of 6.6%, 10%, 15%, 20%, and 23.4% on Fe recovery and P content were studied, and the results shown in Fig. 12.

Fig. 12 shows that the anthracite dosage has a significant effect on the Fe recovery and P content of PRI. At an anthracite dosage of 6.6%, Fe recovery was 33.65 % and the P content was 0.067 %. Furthermore, at an anthracite dosage of 15%, Fe recovery increased to 87.51% and the P content increased to 0.115 %. When the reductant dosage was increased from 15% to 23.4%, Fe recovery increased to 93.81% and the P content increased to 0.26%. This is because, with an increase in the dosage of anthracite, the reducing atmosphere is enhanced, which is favorable for the reduction of iron minerals, consequently increasing Fe recovery. However, the enhancement of the reducing atmosphere would also cause apatite to be reduced and form iron–phosphorus alloys with metallic iron.

Based on the results shown in Figs. 11 and 12, we concluded that, at a reductant dosage of 15%, $\text{Na}_2\text{CO}_3:\text{CaCO}_3 \geq 3:7$, and dephosphorization agent dosage of more than 18% excellent iron extraction and phosphorus reduction can be achieved, with an Fe recovery of $\geq 90\%$ and a P content of $\leq 0.10\%$ in PRI.

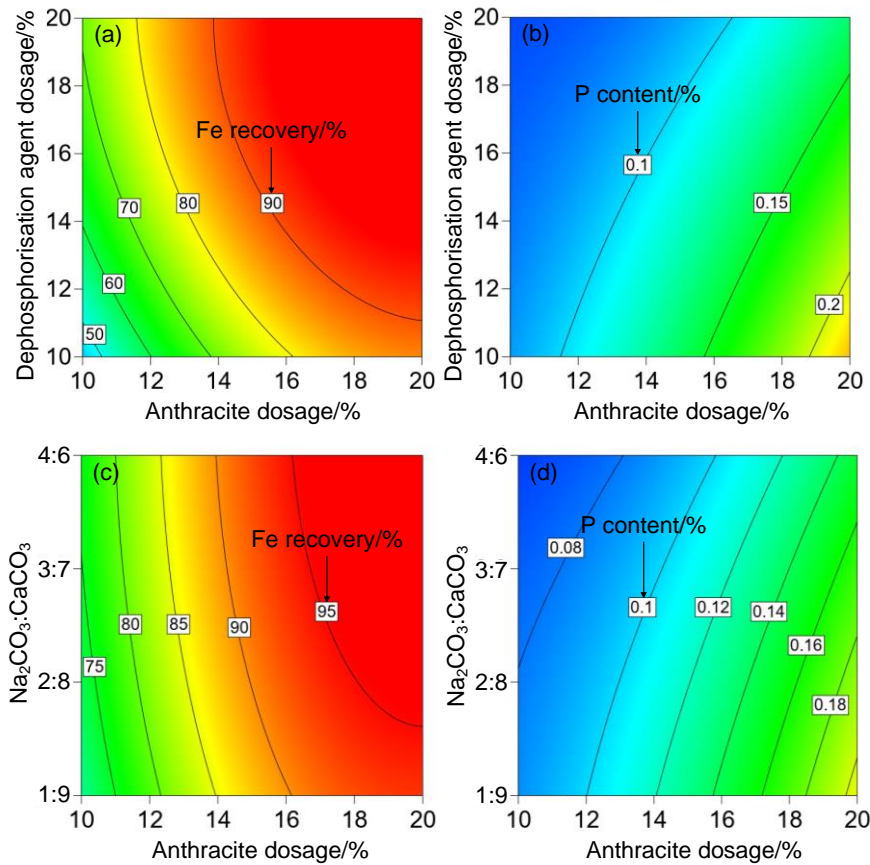


Fig. 11. Effect of the interaction between dephosphorization agent and reductant on PRI: (a), (b) Effect of anthracite and dephosphorization agent dosages on the Fe recovery and P content of PRI, respectively. (c), (d) Effect of anthracite dosage and $\text{Na}_2\text{CO}_3:\text{CaCO}_3$ ratio on the Fe recovery and P content of PRI, respectively

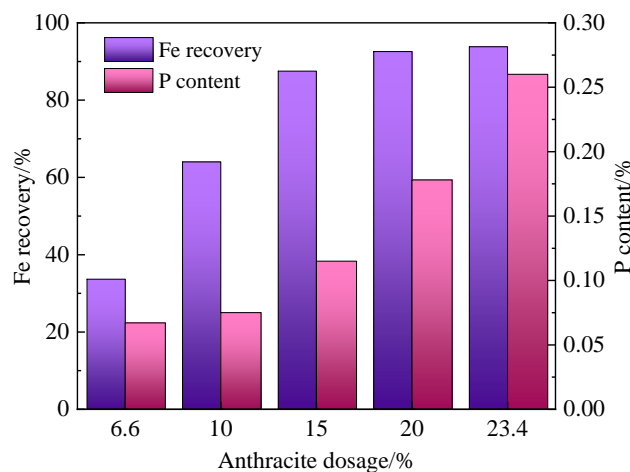


Fig. 12. Effect of anthracite dosage on PRI

4. Conclusions

- (1) In the process of direct reduction of HPOP, Na_2CO_3 and CaCO_3 reacted with Al_2O_3 and SiO_2 , which inhibited the formation of hercynite (FeAl_2O_4) and fayalite (Fe_2SiO_4) and promoted the reduction

- of metallic iron (Fe). Furthermore, the reduction of apatite was inhibited, and the generation of FeP_2 was prevented. The form of phosphorus in the gangue was changed from $\text{Ca}_3(\text{PO}_4)_2$ to $\text{Na}_2\text{Ca}_4(\text{PO}_4)_2\text{SiO}_4$; thus, iron extraction and phosphorus reduction were achieved.
- (2) Under the condition of a certain dosage of the reductant, increasing the dosages of Na_2CO_3 and CaCO_3 and increasing the content of Na_2CO_3 in the dephosphorization agent was found to be beneficial to the growth of metal iron particles and increasing the dosage of the dephosphorization agent of Na_2CO_3 and CaCO_3 had a more significant effect on metal iron particles than increasing the content of Na_2CO_3 in the dephosphorization agent.
 - (3) Increasing the dosage of Na_2CO_3 and CaCO_3 , increasing the content of Na_2CO_3 in the dephosphorization agent, and increasing the dosage of anthracite increased the Fe recovery of PRI. Increasing the dosage of the dephosphorization agent, increasing the content of Na_2CO_3 in the dephosphorization agent, and decreasing the dosage of anthracite gradually decreased the P content of PRI.
 - (4) Under the condition of the reductant dosage of 15%, $\text{Na}_2\text{CO}_3:\text{CaCO}_3 \geq 3:7$, the dosage of the dephosphorization agent of more than 18%, an Fe recovery of $\geq 90\%$ and a P content of $\leq 0.10\%$ from PRI can be achieved.

Acknowledgments

This work was supported by the National Key R&D Program funded project of China (Grant No. 2021YFC2902404).

References

- ANAMERIC, B., KAWATRA, S.K., 2007. *Properties and features of direct reduced iron*. Mineral processing and extractive metallurgy review. 28, 59-116.
- BAO, Q., GUO, L., GUO, Z., 2021. *A novel direct reduction-flash smelting separation process of treating high phosphorous iron ore fines*. Powder Technology. 377, 149-162.
- POWNCBEY, M.I., HAPUGODA, S., MANUEL, J., WEBSTER, N.A.S., MACRAE, C.M., 2019. *Characterisation of phosphorus and other impurities in goethite-rich iron ores – Possible P incorporation mechanisms*. Minerals Engineering. 143, 106022.
- ROY, S.K., NAYAK, D., RATH, S.S., 2020. *A review on the enrichment of iron values of low-grade Iron ore resources using reduction roasting-magnetic separation*. Powder Technology. 367, 796-808.
- SUN, Y., HAN, Y., GAO, P., WEI, X., LI, G., 2015. *Thermogravimetric study of coal-based reduction of oolitic iron ore: Kinetics and mechanisms*. International Journal of Mineral Processing. 143, 87-97.
- JIN, J., ZHOU, W., SUN, Y., HAN, Y., LI, Y., 2021. *Reaction Characteristics and Existing Form of Phosphorus during Coal-Based Reduction of Oolitic Iron Ore*. Minerals. 11, 247.
- WU, S., SUN, T.C., XU, H., 2023. *A new way to efficient utilization of eggshell waste: As green dephosphorization agent and accelerator for reduction roasting of high-phosphorus oolitic iron ore*. Process Safety and Environmental Protection. 173, 702-714.
- WU, S., SUN, T.C., KOU, J., 2022. *A novel and clean utilization of converter sludge by co-reduction roasting with high-phosphorus iron ore to produce powdery reduced iron*. Journal of Cleaner Production. 363, 132362.
- ZHANG, H., LUO, L., 2017. *Process mineralogy and characteristic associations of iron and phosphorus-based minerals on oolitic hematite*. Journal of Central South University. 24, 1959-1967.
- NUNES, A.P.L., PINTO, C.L.L., VALADÃO, G.E.S., VIANA, P.R.D.M., 2012. *Floatability studies of wavellite and preliminary results on phosphorus removal from a Brazilian iron ore by froth flotation*. Minerals Engineering. 39, 206-212.
- OMRAN, M., FABRITIUS, T., MATTILA, R., 2015. *Thermally assisted liberation of high phosphorus oolitic iron ore: A comparison between microwave and conventional furnaces*. Powder Technology. 269, 7-14.
- SUN, Y., HAN, Y., LI, Y., LI, Y., 2017. *Formation and characterization of metallic iron grains in coal-based reduction of oolitic iron ore*. International Journal of Minerals, Metallurgy, and Materials. 24, 123-129.
- TANG, H., QI, T., QIN, Y., 2015. *Production of Low-Phosphorus Molten Iron from High-Phosphorus Oolitic Hematite Using Biomass Char*. JOM. 67, 1956-1965.
- XIAO, J., ZHOU, L., 2019. *Increasing Iron and Reducing Phosphorus Grades of Magnetic-Roasted High-Phosphorus Oolitic Iron Ore by Low-Intensity Magnetic Separation-Reverse Flotation*. Processes. 7, 388.

- CHEN, C., ZHANG, Y., ZOU, K., ZHANG, F., 2023. *Flotation Dephosphorization of High-Phosphorus Oolitic Ore*. Minerals (Basel). 13, 1485.
- DELVASTO, P., VALVERDE, A., BALLESTER, A., MUÑOZ, J.A., GONZÁLEZ, F., BLÁZQUEZ, M.L., IGUAL, J.M., GARCÍA-BALBOA, C., 2008. *Diversity and activity of phosphate bioleaching bacteria from a high-phosphorus iron ore*. Hydrometallurgy. 92, 124-129.
- PAN, J., LU, S., LI, S., ZHU, D., GUO, Z., SHI, Y., DONG, T., 2022. *A New Route to Upgrading the High-Phosphorus Oolitic Hematite Ore by Sodium Magnetization Roasting-Magnetic Separation-Acid and Alkaline Leaching Process*. Minerals (Basel). 12, 568.
- SHEN, S.B., RAO, R.R., WANG, J.C., 2013. *Application of indigenous sulfur-oxidizing bacteria from municipal wastewater to selectively bioleach phosphorus from high-phosphorus iron ore: effect of particle size*. Environmental technology. 34, 173-180.
- WANG, H., LI, G., ZHAO, D., MA, J., YANG, J., 2017. *Dephosphorization of high phosphorus oolitic hematite by acid leaching and the leaching kinetics*. Hydrometallurgy. 171, 61-68.
- ZHANG, L., MACHIELA, R., DAS, P., ZHANG, M., EISELE, T., 2019. *Dephosphorization of unroasted oolitic ores through alkaline leaching at low temperature*. Hydrometallurgy. 184, 95-102.
- WU, S., SUN, T., KOU, J., XU, H., 2023. *A new iron recovery and dephosphorization approach from high-phosphorus oolitic iron ore via oxidation roasting-gas-based reduction and magnetic separation process*. Powder Technology. 413, 118043.
- WU, S., LI, Z., SUN, T., KOU, J., LI, X., 2021. *Effect of additives on iron recovery and dephosphorization by reduction roasting-magnetic separation of refractory high-phosphorus iron ore*. International journal of minerals, metallurgy and materials. 28, 1908-1916.
- YU, W., SUN, T., CUI, Q., 2014. *Can sodium sulfate be used as an additive for the reduction roasting of high-phosphorus oolitic hematite ore?* International Journal of Mineral Processing. 133, 119-122.
- YU, W., SUN, T., CUI, Q., XU, C., KOU, J., 2015. *Effect of Coal Type on the Reduction and Magnetic Separation of a High-phosphorus Oolitic Hematite Ore*. ISIJ International. 55, 536-543.
- WU, S., SUN, T., KOU, J., LI, X., XU, C., CHEN, Z., 2022. *Influence of Sodium Salts on Reduction Roasting of High-Phosphorus Oolitic Iron Ore*. Mineral processing and extractive metallurgy review. 43, 947-953.
- WU, S., LI, Z., SUN, T., LI, X., XU, C., 2022. *Effect of calcium compounds on direct reduction and phosphorus removal of high-phosphorus iron ore*. Journal of Central South University. 29, 443-454.
- XU, H., SUN, T., KOU, J., HAN, W., WU, S.C., 2023. *Effect of Raw Material Particle Size on the Direct Reduction Process of High-Phosphorus Oolitic Hematite*. Mining, metallurgy & exploration. 40, 109-120.
- YU, W., TANG, Q., CHEN, J., SUN, T., 2016. *Thermodynamic analysis of the carbothermic reduction of a high-phosphorus oolitic iron ore by FactSage*. International Journal of Minerals, Metallurgy, and Materials. 23, 1126-1132.
- LI, L., SUN, T., KOU, J., XU, C., LIU, Z., GUO, Q., 2012. *Industry Test on Phosphorus Removal and Direct Reduction of High-phosphorus Oolitic Hematite Ore*. Advanced Materials Research. 402, 535-541.
- LI, L., CHANG, S., HUA, Z., YAN, X., 2012. *Effect of Coal levels during Direct Reduction Roasting of High Phosphorus Oolitic Hematite in a Tunnel Kiln*. International Journal of Mining Science and Technology. 22, 323-328.